Available online at www.sciencedirect.com
ScienceDirect
Journal of the European Ceramic Society 30 (2010) 549–554
www.elsevier.com/locate/jeurceramsoc

Electric force microscopy investigations of barrier formations in ZnO-based varistors

S.M. Gheno *, R.H.G.A. Kiminami, M.R. Morelli, P.I. Paulin Filho

Federal University of Sao Carlos, Department of Materials Engineering, Rod. Washington Luiz, km 235, C. Postal 676, São Carlos 13565-905, SP, Brazil

Available online 7 July 2009

Abstract

The well known metal-oxide varistors (MOVs) are polycrystalline electronic ceramic materials whose electrical behavior is dominated by their grain boundaries. ZnO-based varistors are MOVs whose nonlinear properties are characterized by an electrical resistance that decreases as the applied voltage field increases. The objective of this work was to image the Schottky barriers in ZnO doped with 0.5 mol.% Cu and x wt.% G (G is a frit and $x = 0$, 1 and 5%). The frit is used to form a glassy insulating layer around grain boundaries. Samples were sintered at 850 °C and the microstructures were analyzed by atomic force microscopy (Nanoscope IIIa, VEECO Instruments). Electric force microscopy (EFM) experiments were conducted to map the electric field distribution on the surface of CuO–ZnO-based varistors. The formation of Schottky barriers was observed and their width measured.

Keywords: Grain boundaries; Electrical properties; Varistors; ZnO

1. Introduction

Ceramic materials with electrical and electronic properties have been investigated extensively in response to the increasing demand for these materials by the electronic and microelectronic industries.[1–4] The applications and use of several technologically important ceramic materials, such as varistors,[1–5] thermistors (PTCR),[4,5] capacitors,[4,5] gas sensors[4–6] and catalysts,[7–9] are controlled by phenomena associated with grain boundaries. These materials are used in temperature control, surge protection, humidity sensors, and gas sensing devices.[3,10]

Varistors or surge suppressors are electrical devices that have a nonlinear current–voltage relation which is used to limit voltage transients in line transmission and electronic circuits.[4,7,11,12] These devices, which have microstructures with n-type semiconductor grains and insulating grain boundaries, use materials such as ZnO,[7,13] $SrTiO_3$,[14] TiO_2,[15] WO_3[16] and SnO_2.[17] Varistor technology has improved considerably in the last three decades through advanced processing techniques and high quality materials.[18]

Because they are polycrystalline materials, varistors have a high concentration of surface and structural electronic defects. The type and amount of defects are related to the various processing steps they undergo during the fabrication process. These systems have conductive grains connected by an insulating interface that controls their nonlinear behavior. The stability of such devices derives from the stability of grain boundaries, which are affected by the selection and uniform distribution of dopants along grain boundaries and by the chemistry of the grain boundaries.[19] The uniform distribution of dopants at grain boundaries leads to a high number of active barriers and enhanced properties.[4,18,20,21]

ZnO ceramic varistors have a complex microstructure, which makes their processing and the control of their electrical characteristics difficult, such as high nonlinear behavior, fast response to voltage transients, protection level close to operating voltages, high energy absorption, low loss currents and low residual voltages, used in the protection of electrical circuits, electronic equipment and high voltage systems.[22,23] The characteristics that allow for their applications are the potential barriers that form at their grain boundaries, which result in the nonlinear behavior of current–voltage curves.

In this investigation, electrical force microscopy (EFM) was employed to analyze the potential barrier in local potential measurements of varistors of ZnO–CuO–frit through surface imaging. The investigation and mapping of the distribution of

* Corresponding author. Tel.: +55 16 3351 8790; fax: +55 16 3361 5404.
E-mail address: gheno@dema.ufscar.br (S.M. Gheno).

0955-2219/$ – see front matter © 2009 Elsevier Ltd. All rights reserved.
doi:10.1016/j.jeurceramsoc.2009.05.039

potential barriers across the ZnO–CuO–frit surface was carried out using atomic force microscopy (AFM)/EFM, varying the applied potential on the sample surface. Images of potential barriers were obtained through changes in tip frequency associated with changes in grain boundary regions.

2. Experimental

The powders of ZnO varistors and sintered samples were prepared by the lyophilization process, as described by Bellini et al.[24] Pellets were produced by pressing the powders at 75 MPa in a uniaxial press without pressing additives and sintering in air at 850 °C for 1 h. Pellet (a), with a 5 mm diameter and 3 mm thickness, was used for AFM/EFM characterization, and pellet (b), with the same diameter but with a thickness of 1 mm, was used for the analysis of electrical properties.

For purposes of identification, the samples were given the following specific names—ZnO–CuO: ZnO + 0.5 wt.% Cu; ZnO–CuO–G_1: ZnO + 0.5 wt.% Cu + 1 wt.% frit; and ZnO–CuO–G_5: ZnO + 0.5 wt.% Cu + 5 wt.% frit. The frit was prepared as follows: a batch of precursor oxides and isopropyl alcohol was mixed in a ball mill mixer with zirconia mixing media for 4 h. The oxide powders were batched in the following proportions: 26 wt.% SiO_2 + 62 wt.% PbO + 7 wt.% B_2O_3 + 5 wt.% ZnO. The powder mixture was dried at 110 °C for 24 h and disaggregated prior to melting at 900 °C in a conventional furnace and fritting in distilled water.

The ZnO, ZnO + 0.5 mol.% Cu powders and the crystalline phases of sintered samples of ZnO + 0.5 mol.% Cu + x mol% G (x = 0, 1, and 5) samples were analyzed by X-ray diffraction (XRD) using a Siemens diffractometer (D 5005) with Cu-α radiation, 50 kV voltage, and 100 mA current.

The durability of varistors is related directly to the ion polarization state at the grain boundaries, creating the potential barrier. This polarization state is related to ion diffusion. The potential barrier was analyzed using an atomic force microscope (Nanoscope IIIA, Digital Instruments) operating in the electric force microscopy (EFM) mode and equipped with an electronic extender module (Veeco Instruments, Santa Barbara, CA). Topographical measurements and electrical data were obtained by the two-pass technique (Lift Mode). In this configuration, during the first pass, the probe operates in Tapping Mode to scan a topographical line. In the second scan, the cantilever is lifted to a predefined distance (75 nm) in order to minimize the effect of the van der Waals forces, during which it detects the variations in the electrical force gradient over the same line and the influence of surface topography is ruled out.[25–28] An NSC15 tip (MikroMasch) was used in all the experiments. Electrostatic force gradient images were obtained by monitoring the shifts in phase and frequency. The images of surface potential and barrier layer were obtained by applying 4 and 8 V *in situ* to the sample. Imaging was carried out at room temperature.

3. Results and discussion

Fig. 1 shows the powder XRD spectra of crushed pellets obtained from samples of ZnO (Fig. 1(a)) and ZnO + 0.5 mol.% Cu (Fig. 1(b)) sintered in air at 850 °C for 1 h. Fig. 2 depicts the XRD spectra of ZnO–CuO (a), ZnO–CuO–G_1 (b), and ZnO–CuO–G_5 (c) pellets sintered in air at 850 °C for 1 h. A comparison with the powder diffraction files (PDF) of the Joint Committee on Powder Diffraction Standards (JCPDS) revealed only the ZnO phase. No Cu peak is visible in either Fig. 1 or Fig. 2 due to the low Cu content. The XRD peaks (2θ = 26.7° and 34°) showed a new phase, Zn_2SiO_4, resulting from the reaction of the vitreous phase at high temperature with the zinc grains in both ZnO–CuO–G_1 and ZnO–CuO–G_5. However, the amount of Zn_2SiO_4 phase did not suffice to modify the properties of the ZnO–CuO–G_x varistor system. The decrease in peak intensity with increasing frit content shown in Fig. 2 was attributed to the 'diluting effect' of the amorphous phase that was introduced.

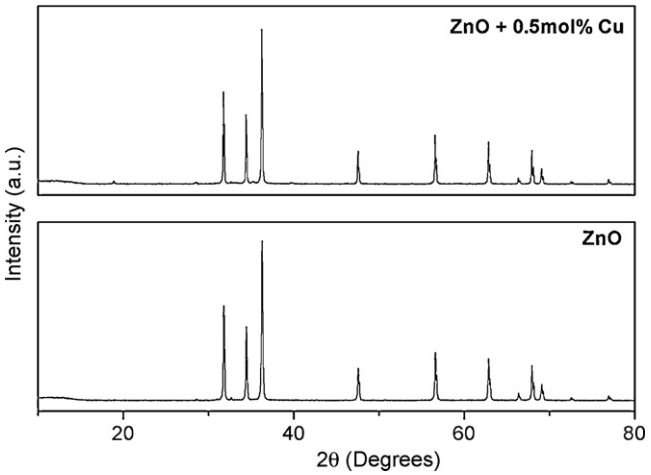

Fig. 1. Powder XRD obtained from samples of ZnO (a) and ZnO + 0.5 mol.% Cu (b).

Fig. 3 *J–E* presents the curves of ZnO–CuO, ZnO–CuO–G_1, and ZnO–CuO–G_5 samples sintered in air at 850 °C for 1 h. The progressive increase in the frit (ZnO–CuO–G_5) concentration modified the sample's resistivity and the varistor effect.

Figs. 4–6 show the combined AFM and EFM results. Figs. 4(a), 5(a), and 6(a) give topographic information, show-

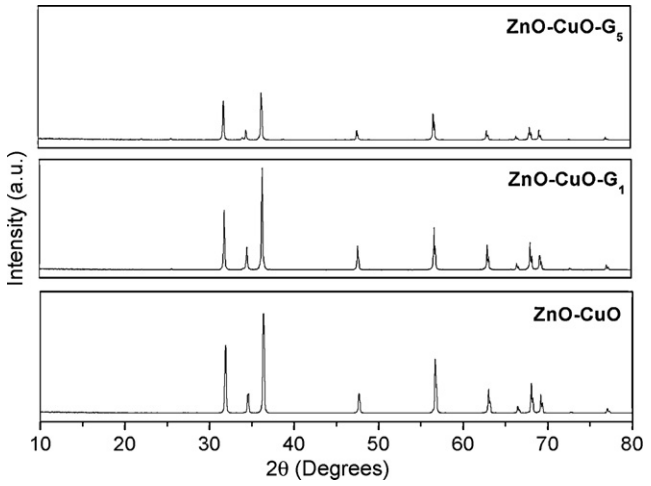

Fig. 2. XRD obtained from samples: ZnO–CuO (a), ZnO–CuO–G_1 (b), and ZnO–CuO–G_5 (c).

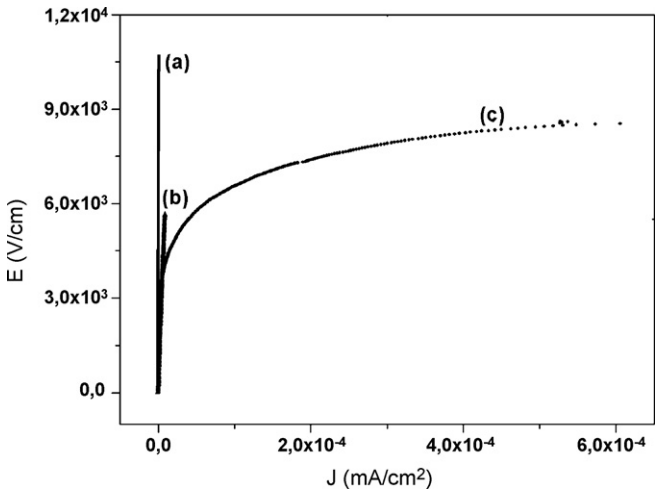

Fig. 3. The current density versus electric field (*J–E*) curves of samples: ZnO–CuO (a), ZnO–CuO–G_1 (b), and ZnO–CuO–G_5 (c).

ing pores (black regions). It was also observed that the grain geometry and diameter differ considerably (1–3 μm). The grain size can be controlled by sintering temperature and time and also by different additives, as reported by Bellini et al.[24,29–31] These images indicate that densification was not complete due to the presence of pores (Fig. 4a). Moreover, it was found that there was a reduction in grain size only after the addition of the frit, but the increase in frit content did not change the grain size. The porosity and nonuniformity of grain size distribution can increase the leakage current, favoring electrical degradation. In varistors, the leakage current decreases as the grain size decreases, although doped ZnO varistors of small size have a large leakage current.[24,29–31]

The EFM images of the ZnO–CuO, ZnO–CuO–G_1, and ZnO–CuO–G_5 varistors depicted in Figs. 4(b, c), 5(b, c), and 6(b, c), respectively, were obtained with a dc bias voltage ranging from 4 and 8 V. These images indicate that increasing the bias tip voltage causes the concentration of negative charges stored in the grain boundary region to increase. The charge accumulation observed in the grain boundary region indicates the presence of active potential barriers. The grain boundary is visible at 4 V, as indicated by the topographic image. The dark regions, which were attributed to semiconducting material, indicate that the grains are conductive. The bright regions, especially at the grain boundaries, were ascribed to the electrostatic charge produced by the potential barrier.

The results presented in the EFM images show that increasing the applied voltage increases the concentration of negative loads at the grain boundary, indicating the presence of effective (or attractive) potential barriers. The EFM images record the potential barriers found at the grain boundaries. The electrical current in varistors follows the path of least resistance, or the routes with fewer borders (or larger grains) and those with smaller grain boundary barriers. Uniform grain sizes allow more electric current to pass through many parallel paths. The effects of porosity and nonuniform grain distribution should therefore be avoided.

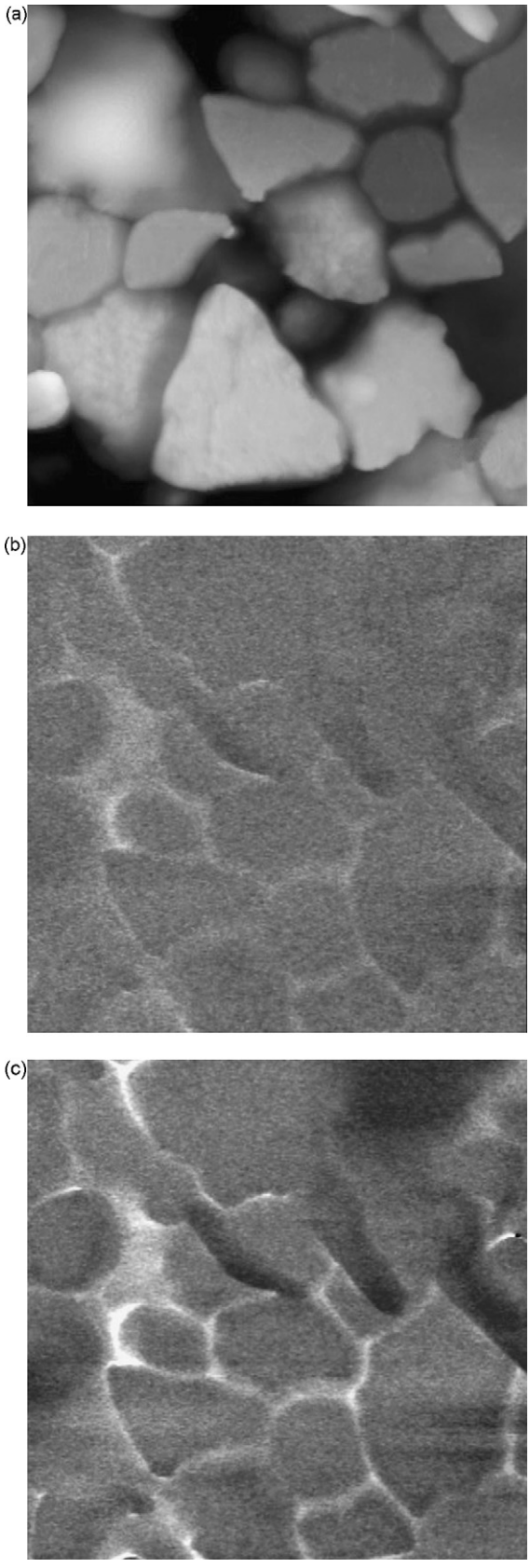

Fig. 4. Analysis of ZnO–CuO sample. Topography (7.5 μm × 7.5 μm × 0.45 μm) (a); profiles EFM with application of external voltage (7.5 μm × 7.5 μm): 4 V (b), 8 V (c).

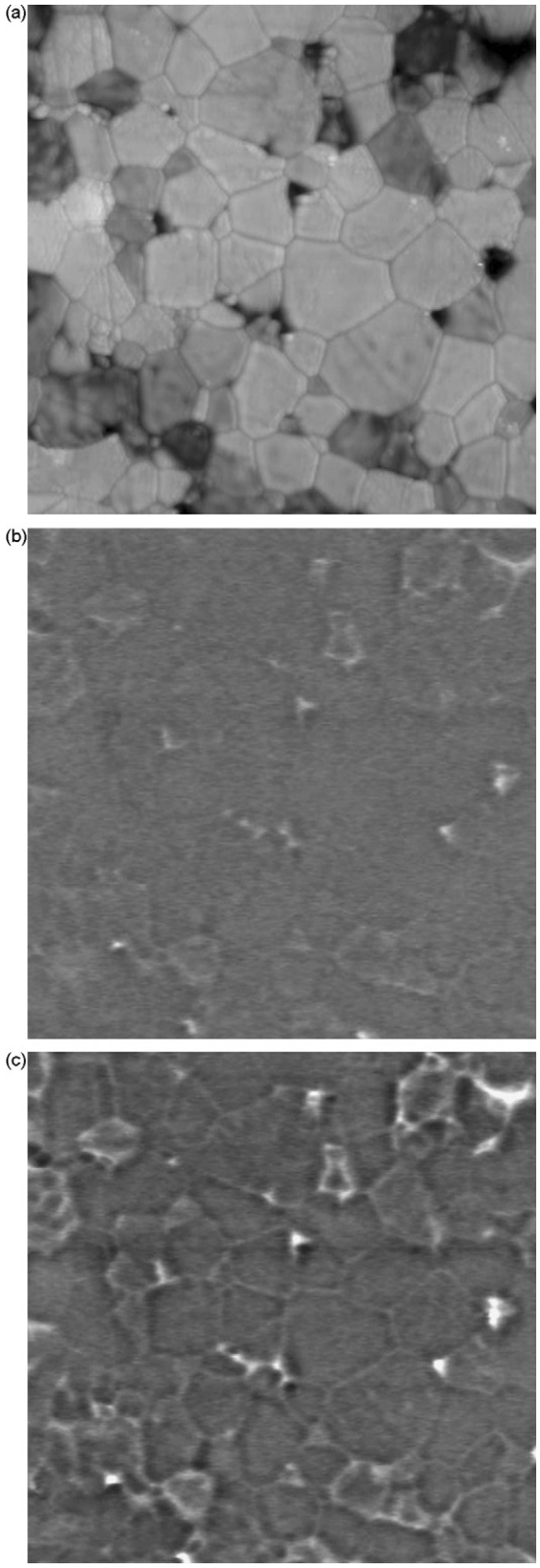

Fig. 5. Analysis of ZnO–CuO–G_1 sample. Topography (7.5 μm × 7.5 μm × 0.45 μm) (a); profiles EFM with application of external voltage (7.5 μm × 7.5 μm): 4 V (b), 8 V (c).

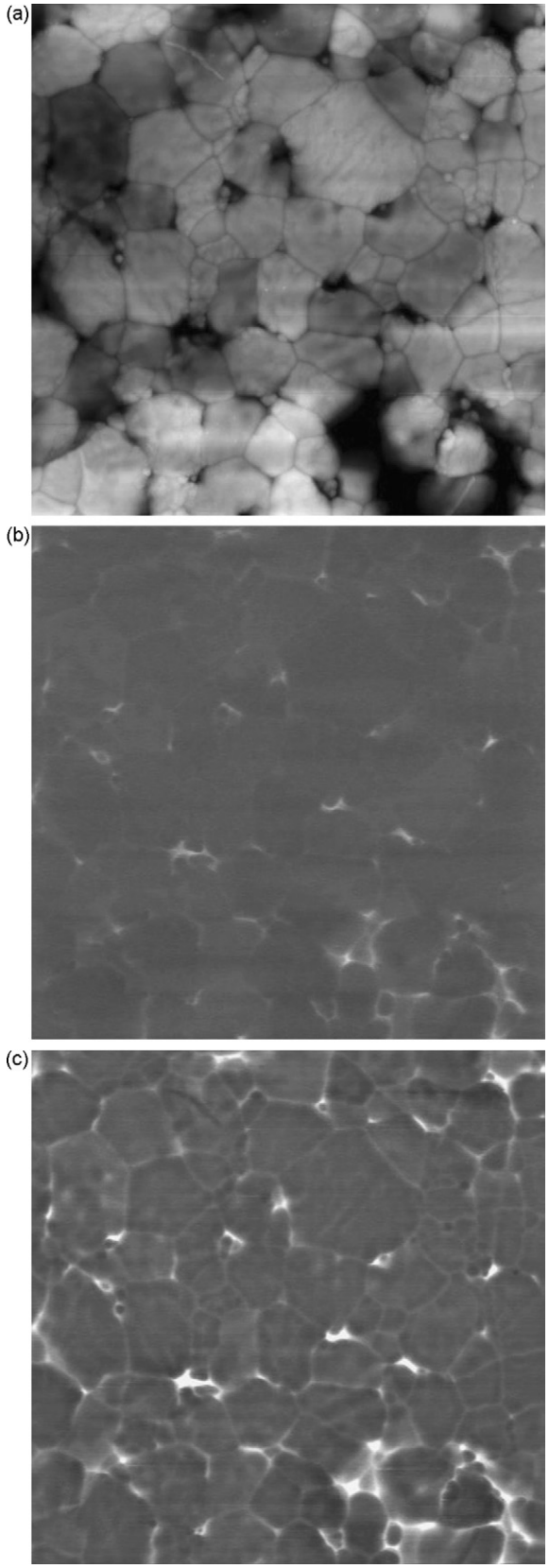

Fig. 6. Analysis of ZnO–CuO–G_5 sample. Topography (7.5 μm × 7.5 μm × 0.45 μm) (a); profiles EFM with application of external voltage (7.5 μm × 7.5 μm): 4 V (b), 8 V (c).

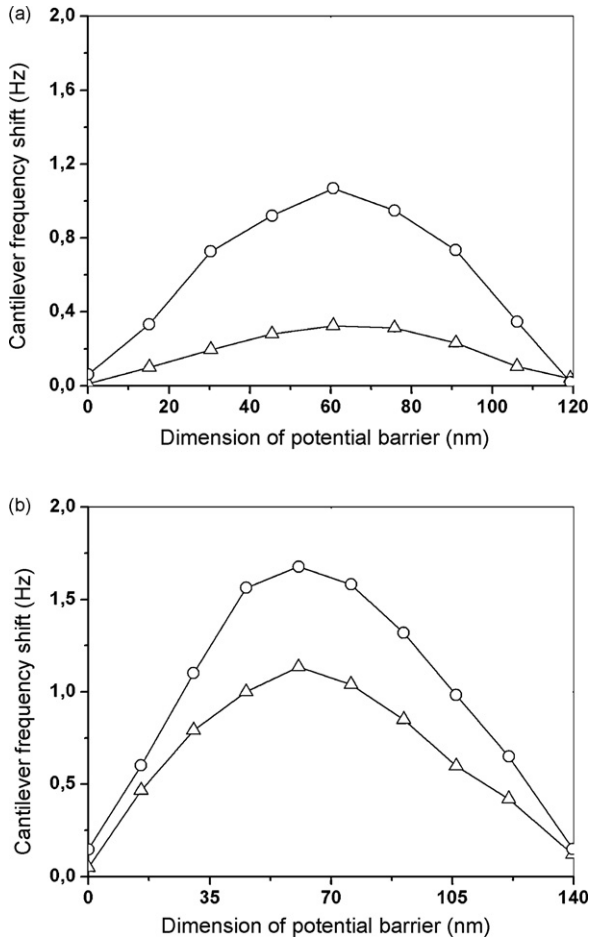

Fig. 7. Dimension of potential barrier of ZnO–CuO–G_1 (a), and ZnO–CuO–G_5 (b): 4 V (Δ) and 8 V (◯).

The surface potential clearly identifies a grain boundary, as shown in Fig. 7. Potential profiles were extracted from various positions along the grain boundaries in all the samples. Based on these profiles, the dimensions of the potential barriers at the grain boundaries were determined at 120 nm for ZnO–CuO–G_1 (Fig. 7(a)) and at 140 nm for ZnO–CuO–G_5 (Fig. 7(b)). These results indicate that increasing the frit content to 5% caused the width of the potential barrier to increase. The width of the resistive layer, which is a function of the material's chemistry and processing, is not expected to be very sensitive to the applied voltage, as indicated in Fig. 7(a and b). One possible explanation for this behavior is that the contribution of the applied voltage to the conductivity of the glassy phase increases as the amount of this voltage increases. The potential barrier increases in width for the same reason, while the conductivity at the breakdown voltage decreases due to the substantial contribution of the glassy phase to the material's conductivity.

Grain boundaries have been found to give rise to nonlinear current/voltage characteristics by forming barriers against electrical conduction. In polycrystalline materials in general, most grain boundaries grow randomly and are low-symmetry, high-angle grain boundaries. The basic concept underlying varistor action is that the current/voltage characteristics are controlled by the existence of electrostatic barriers at the interfaces between grains. The origin of these barriers is an interface charge stemming from lattice mismatch, defects and dopants at the grain boundary. The interface charge changes the Fermi level in the vicinity of the grain boundary, resulting in band bending. The electronic charges stored at an interface represent a repulsive potential for the majority of carriers – the electrons in the case of an n-doped semiconductor – across the interface.

Potential barrier height and width are both associated with an increase in the number of electrons and holes in the grain and grain boundary regions. The amount of trapped electrons in the grain boundary regions, resulting from the segregation of dopants next to the grain boundaries, as well as the creation of positive defects in the depletion layer ($VO^{\bullet\bullet}$) and negative defects at the interfaces (metallic vacancies), are also related to the potential barrier characteristics. Thus, increases in potential barrier can be associated with increased effective grain boundary states.

4. Conclusions

The use of atomic force microscopy operating in the electric force microscopy mode is a powerful tool for analyzing phenomena associated with grain boundary regions in varistors. The potential barriers formed at grain boundaries due to the segregation of dopants in these regions, as reported in the literature, were successfully imaged *in situ*. The potential profiles indicated that the increase of frit content to 5% was responsible for the increase in the potential barrier width from 120 nm to 140 nm.

Acknowledgements

The authors gratefully acknowledge the Brazilian agencies FAPESP and CAPES for their financial support of this work. We are also indebted to the LNLS (Brazilian Synchrotron Light Laboratory) in Campinas, SP, Brazil for the AFM/EFM analyses.

References

1. Cássia-Santos, M. R., Sousa, V. C., Oliveira, M. M., Sensato, F. R., Bacelar, W. K., Gomesa, J. W. *et al.*, Recent research developments in SnO_2-based varistors. *Mater. Chem. Phys.*, 2005, **90**(1), 1–9.
2. Cássia-Santos, M. R., Sousa, V. C., Oliveira, M. M., Bueno, P. R., Bacelar, W. K., Orlandi, M. O. *et al.*, SnO_2 and TiO_2 based electronic ceramics. *Cerâmica*, 2001, **47**, 136–143.
3. Brito, S. L. M., Gouvêa, D. and Ganzella, R., Study of polyacrylate adsorption in a commercial varistor system: characterization of the physical-chemistry properties. *Cerâmica*, 2005, **51**, 30–36.
4. Hozer, L., *Semiconductor Ceramics: Grain Boundary Effects*. Ellis Horwood/Polish Scientific Publishers, West Sussex, England, 1994.
5. Hwang, C.-C. and Wu, T.-Y., Synthesis and characterization of nanocrystalline ZnO powders by a novel combustion synthesis method. *Mater. Sci. Eng. B*, 2004, **111**, 197–206.
6. Gupta, T. K., Tressler, R. E., Messing, G. L., Pantino, C. G. and Newhan, R. H., *Tailoring Multiphase and Composite Ceramics*. Plenum Press, New York, 1986, pp. 439–507.
7. Gupta, T. K., Application of Zinc Oxide Varistors. *J. Am. Ceram. Soc.*, 1990, **73**(7), 1817–1840.
8. Farrauto, R. J. and Heck, R. M., Environmental catalysis into the 21st century. *Catal. Today*, 2000, **55**, 179–187.

9. Mills, A. and Hunt, S. L., An overview of semiconductor photocatalysis. *J. Photochem. Photobiol. A: Chem.*, 1997, **108**(1), 1–35.
10. Buchnan, R. C., *Ceramic Materials for Electronics—Processing, Properties, and Applications*. Marcel Dekker Inc, New York, USA, 1986, p. iii.
11. Wang, M.-H., Hu, K.-A., Zhao, B.-Y. and Zhang, N.-F., Electrical characteristics and stability of low voltage ZnO varistors doped with Al. *Mater. Chem. Phys.*, 2006, **100**(1), 142–146.
12. Levinson, L. M. and Philipp, H. R., Zinc oxide varistors—a review. *Am. Ceram. Soc. Bull.*, 1986, **65**(4), 639–646.
13. Matsuoka, M., Nonohmic Properties of Zinc Oxide Ceramics. *Jpn. J. Appl. Phys.*, 1971, **10**(6), 736–746.
14. Yamaoka, N., Masuyama, M. and Fukui, M., $SrTiO_3$-based boundary-layer capacitor having varistor characteristics. *Am. Ceram. Soc. Bull.*, 1983, **62**(6), 698–700.
15. Yan, M. F. and Rhodes, W. W., Preparation and properties of TiO_2 varistors. *Appl. Phys. Lett.*, 1982, **40**, 536–537.
16. Makarov, V. and Tontelj, M., Novel varistor material based on tungsten oxide. *J. Mater. Sci. Lett.*, 1994, **13**, 937–939.
17. Pianaro, S. A., Bueno, P. R., Longo, E. and Varela, J. A., A new SnO_2-based varistor system. *J. Mater. Sci. Lett.*, 1995, **14**(10), 692–694.
18. Li, S., Xie, F., Liu, F., Li, J. and Alim, M. A., The relation between residual voltage ratio and microstructural parameters of ZnO varistors. *Mater. Lett.*, 2005, **59**, 302–307.
19. Lu, G. Q., *Nanoporous Materials: Science and Engineering*. Imperial College, London, 2001, p. 700.
20. Rittner, M., Market analysis of nanostructured materials. *Am. Ceram. Soc. Bull.*, 2002, **81**(3), 33–36.
21. Matsuoka, M., Masuyama, T. and Iida, Y., Voltage nonlinearity of zinc oxide ceramics doped with alkali earth metal oxide. *Jpn. J. Appl. Phys.*, 1969, **8**, 1275–1276.
22. Ling, H. C., Yan, M. F. and Rhodes, W. W., Monolithic device with dual capacitor and varistors functions. *J. Am. Ceram. Soc.*, 1989, **72**(7), 1274–1276.
23. Schwing, U. and Hoffmann, B., Model experiments describing the microcontact of ZnO varistors. *J. Appl. Phys.*, 1985, **57**(12), 5372–5379.
24. Bellini, J. V., Morelli, M. R. and Kiminami, R. H.G. A., Varistores de ZnO–CuO–Vidro, PI0204858-2 (2002).
25. Sarid, D., *Scanning Force Microscopy with applications to Electric, Magnetic, and Atomic Forces*. Oxford University Press, New York, 1991, pp. 129–151.
26. Magonov, S. N. and Whangbo, M. H., *Surface Analysis with STM and AFM—Experimental and Theoretical Aspects of Image Analysis*. VCH, Weinheim, New York, 1996, pp. 116–128.
27. Meyer, E., Hug, H. J. and Bennewitz, R., *Scanning Probe Microscopy—The Lab on a Tip*. Springer, New York, 2003, p. 29.
28. Gheno, S. M., Hasegawa, H. L. and Paulin Filho, P. I., Direct observation of potential barrier behavior in yttrium–barium titanate observed by electrostatic force microscopy. *Scripts Mater.*, 2007, **56**(6), 545–548.
29. Bellini, J. V., Morelli, M. R. and Kiminami, R. H. G. A., Ceramic system based on ZnO–CuO obtained by freeze-drying. *Mater. Lett.*, 2003, **57**, 3775–3778.
30. Bellini, J. V., Morelli, M. R. and Kiminami, R. H. G. A., Electrical properties of polycrystalline ZnO:CuO obtained from freeze-dried ZnO + copper (II) acetate powders. *J. Mater. Sci.: Mater. Electr.*, 2002, **13**(8), 485–489.
31. Bellini, J. V., Morelli, M. R. and Kiminami, R. H. G. A., Physical changes of sintered ceramics obtained from freeze-dried $ZnO + (CH_3COO)_2Cu{\cdot}H_2O$ powders. *Mater. Lett.*, 2003, **57**, 3325–3329.